High-resolution Photo-excitation Measurements Exacerbate the Long-standing Fe XVII-Oscillator-Strength Problem: Supplemental Material

I. EXPERIMENT AND DATA ANALYSIS

TABLE I. Comparison between experimental values and theoretical predictions of the $3C/3D$ oscillator strength ratio and relative line energy positions achieved within this work.

	Experiment	CI	MCDHF	AMBiT
3C/3D oscillator strength ratio	$3.09(8)_{\rm sys}(6)_{\rm stat}$	3.55(5)	3.55(5)	3.59(5)
Energy 3C (eV)		825.67	825.88(5)	825.923
Energy 3D (eV)		812.22	812.44(5)	812.397
ΔEnergy 3C-3D (eV)	13.398(1)	13.44(5)	13.44(5)	13.526
ΔEnergy 3D-C (eV)	0.1543(13)			
Natural linewidth 3C (meV)		14.74(3)	14.75(3)	14.90
Natural linewidth 3D (meV)		4.02(5)	4.01(6)	4.04

A. Individual methods data and their uncertainities

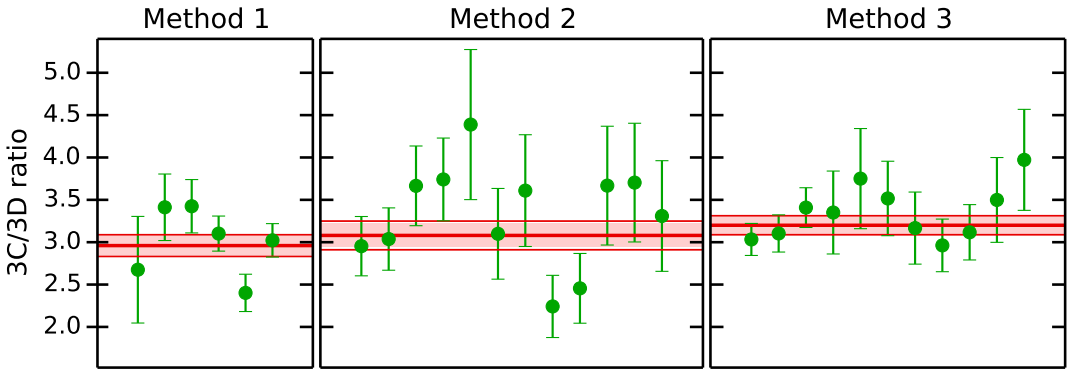

FIG. 1. Experimental 3C/3D ratio for the three different methods. The individual measurements are shown as solid green circles. The weighted mean experimental values and associated 1-σ statistical and systematic uncertainties are indicated as red band.

TABLE II. $3C/3D$ oscillator strength ratios obtained from three diffferent measurement methods and their statistical and systematic uncertainties.

	Method 1	Method 2	Method 3
$3C/3D$ oscillator strength ratio	2.960	3.080	3.210
Uncertainty Budget			
Statistical	0.106	0.140	0.095
Systematics due to:			
(1) ROI width selection on 2D histogram (Fig. 2 of the main paper)	0.030		
(2) ROI centroid selection on 2D histogram	0.044		
(3) Filter transmission and efficiency of the detector	0.030	0.031	0.032
(4) Time-dependent background variation due to the electron-impact excitation	0.036		
(5) Monochromator shifts in the (set) energy position		0.092	
(6) Linewidth constraints in Gaussian fits			0.048
Total systematic uncertainty	0.071	0.097	0.058
Total (statistical + systematic) uncertainties	0.127	0.170	0.111
Common systematics for all three methods:			
Flux variation of the incident photon beam at P04/PETRA III		0.0618	
Final $3C/3D$ oscillator strength ratio	**3.09** $\pm$ **0.08**$_{\text{stat.}}$ $\pm$ **0.06**$_{\text{sys.}}$		

B. Resolving Fe XVII 3D and Fe XVI C lines

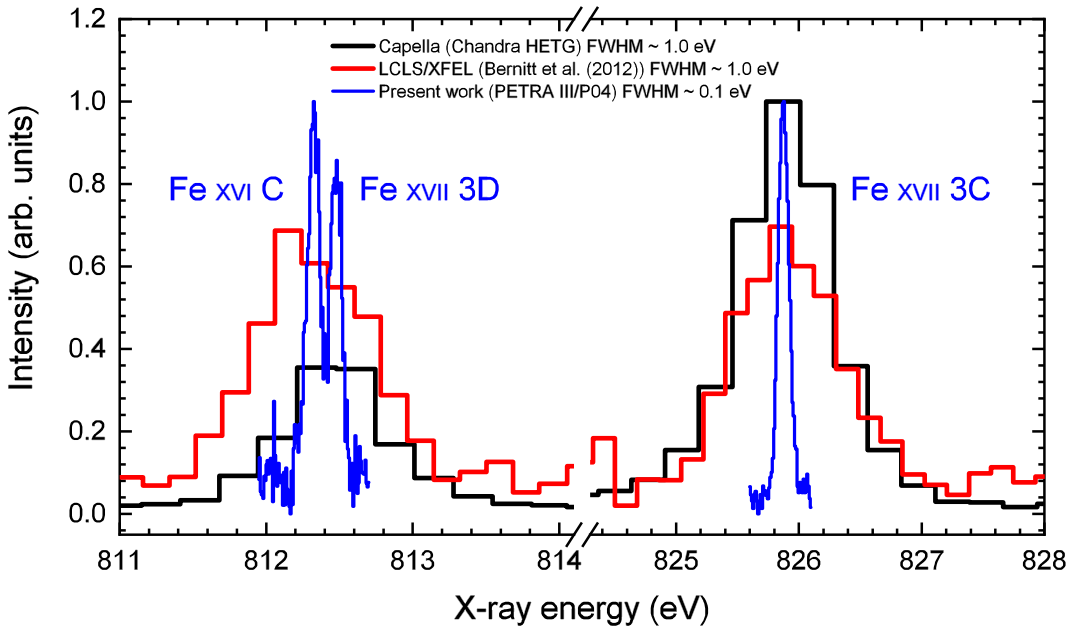

FIG. 2. Spectral resolution comparison between the present work at PETRA III/P04, our previous work at LCLS/XFEL [1], and the high resolution *Chandra* High Energy Transmission Grating (HETG) [2] spectrum of Capella [ObsId: 1103]. In this work, for the first time, we have resolved previously-blended Fe XVI C from Fe XVII 3D line, which are 154.3(1.3) meV apart from each other. This enables us to obtain the line intensity ratio of Fe XVII 3C and 3D without having to subtract the contribution of the Fe XVI C line, in contrast to all other previous works. Moreover, this has largely reduced the systematic uncertainties and eliminated the need for taking resonance-induced population transfer [3] into account, which may have affected the accuracy of our LCLS work [1].

C. Comparison between experimental data, theoretical predictions and astrophysical observations

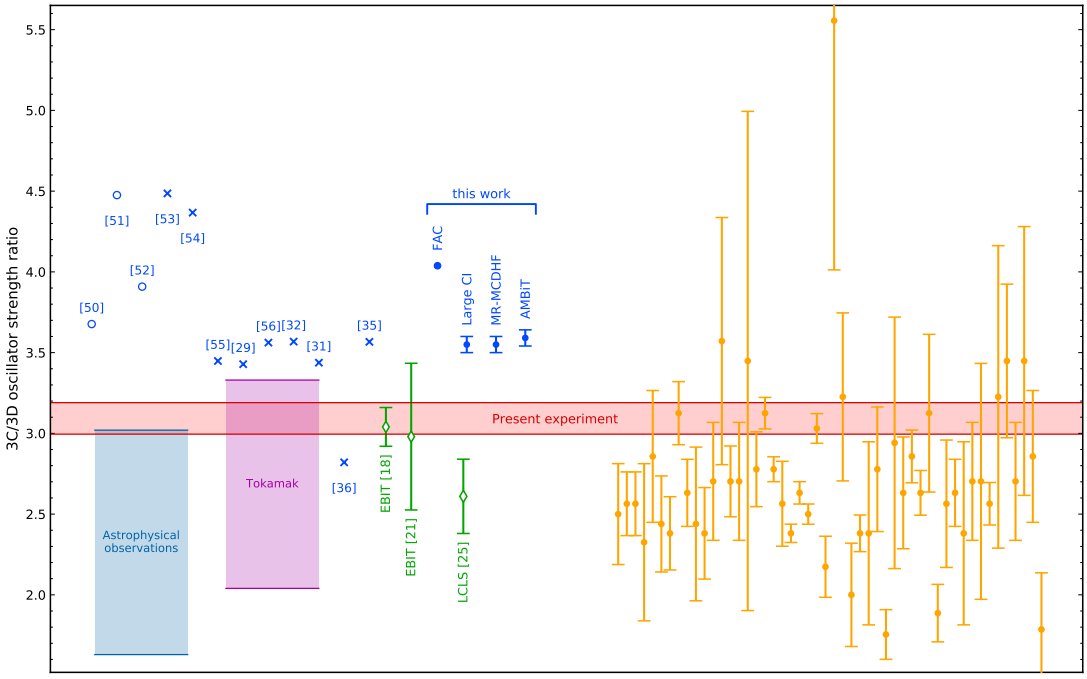

FIG. 3. Present experimental 3C/3D ratios – combined results of three different methods (red band), compared with previous predictions and experiments. Blue open circles: Values from spectral databases. Blue crosses: theoretical predictions. Blue solid circles: our present FAC [4, 5], large-scale CI (Sec. II A), MR-MCDHF (Sec. II B)), and AMBiT (Sec. II C) calculations. Open green diamonds: previous EBIT results. Purple band: spread of Tokamak results [6]. Light blue band: range of ratios observed in the Sun [7, 8], Capella [9, 10], and NGC4636 [11]. Orange solid circles: 46 astrophysical observations of 26 stellar coronae [12] sampled by the RGS onboard *XMM-Newton* and the LETGS/HETGS onboard *Chandra* observatories. Note that the numbers in the square bracket corresponds to the references cited in the main paper.

D. Estimation of photon peak intensity on sample at P04 PETRA III

For an estimation of the photon beam intensity on the plasma sample, we refer to the technical parameters of beamline P04 [13] and generously assume a total time-averaged photon flux after monochromatization of the beam of $\Phi_{\mathrm{Beam}} = 4 \times 10^{12}$ photons/s, a focal spot size of $1 \times 10^{-6}\,\mathrm{cm}^2$, and a photon energy of 825 eV. The 16 ns pulse separation ensures that the upper state population has sufficient time to completely relax into the ground state in between the pulses. We obtain a total energy per bunch of

$$E_{\mathrm{bunch}} \approx 8.5 \times 10^{-6}\,\mathrm{J\,cm^{-2}}. \tag{1}$$

Combined with the typical pulse duration of 44 ps given by the official PETRA III datasheet (see [14] and [15]), we deduce an average intensity per pulse of

$$I \approx 1.9 \times 10^{5}\,\mathrm{W\,cm^{-2}}. \tag{2}$$

For typical pulse shapes, the peak intensity can be expected to be well below $1 \times 10^{6}\,\mathrm{W\,cm^{-2}}$.

II. CALCULATIONS OF 3C AND 3D OSCILLATOR STRENGTHS

A. Very large-scale CI calculations

We start from the solution of the Dirac-Hartree-Fock equations in the central field approximation to construct the one-particle orbitals. The calculations are carried out using a configuration interaction (CI) method, correlating all 10 electrons. The Breit interaction is included in all calculations. The QED effects are included following Ref. [16]. The basis sets of increasing sizes are used to check for convergence of the values. The basis set is designated by the highest principal quantum number for each partial wave included. For example, $[5spdf6g]$ means that all orbitals up to $n = 5$ are included for the $spdf$ partial waves and $n = 5, 6$ orbitals are included for the g partial waves. We find that the inclusion of the $6, 7h$ orbitals does not modify the results of the calculations and omit higher partial waves. The CI many-electron wave function is obtained as a linear combination of all distinct states of a given angular momentum J and parity [17]:

$$\Psi_J = \sum_i c_i \Phi_i \,. \tag{3}$$

The energies and wave functions are determined from the time-independent multiparticle Schrödinger equation $H\Phi_n = E_n\Phi_n$.

We start with all possible single and double excitations to any orbital up to $5spdf6g$ from the $2s^22p^6$, $2s^22p^53p$ even and $2s^22p^53s$, $2s^22p^53d$, $2s2p^63p$, $2s^22p^54d$, $2s^22p^55d$ odd configurations, correlating 8 electrons. We verified that inclusion of the $2s2p^63s$, $2s^22p^54f$, $2s^22p^55f$ even and $2s2p^64p$, $2s^22p^54s$, and $2s^22p^55s$ odd configurations as basic configurations have negligible effect on either energies of relevant matrix elements.

The only unusually significant change in the ratio, by 0.07, is due to the inclusion of the $2s^22p^33d^3$ and $2p^53d^3$ configurations. These are obtained as double excitations from the $2s^22p^53d$ odd configuration, prompting the inclusion of the $2s^22p^54d$, $2s^22p^55d$ to the list of the basic configurations.

Contributions to the energies of Fe^{16+} calculated with different size basis sets and a number of configurations are listed in Table III. The results are compared with experimental data from the NIST database [18] and from a revised analysis of the experimental data [19]. We use LS coupling and NIST data term designations for comparison purposes, but note that jj coupling would be more appropriate for this ion. Contributions to the E1 reduced matrix elements

TABLE III. Contributions to the energies of Fe^{16+} calculated with increased size basis sets and a number of configurations. The results are compared with experiment. All energies are given in cm^{-1} with exception of the last line that shows the difference of the 3C and 3D energies in eV. The basis set is designated by the highest quantum number for each partial wave included. For example, $12spdfg$ means that all orbitals up to $n = 12$ are included for $spdfg$ partial waves. Contributions from triple excitations, excitations from the $1s^2$ shells, and QED contributions are given separately.

Configuration		Expt. [18]	Expt. [19]	$[5spdf6g]$	Triples	$1s^2$	$+[12spdfg]$	$+[17dfg]$	QED	Final	Diff. [18]	Diff. [19]	Diff. [19]
$2p^6$	$^1S_0$	0	0	0	0	0	0	0	0	0	0	0	
$2p^53p$	$^3S_1$	6093450	6093295	6087185	6	254	3876	772	67	6092159	1291	1136	0.02%
$2p^53p$	$^3D_2$	6121690	6121484	6116210	-21	24	2886	701	43	6119842	1848	1642	0.03%
$2p^53p$	$^3D_3$	6134730	6134539	6129041	-23	25	3015	711	94	6132864	1866	1675	0.03%
$2p^53p$	$^1P_1$	6143850	6143639	6138383	-11	41	2825	704	82	6142025	1825	1614	0.03%
$2p^53s$	2	5849490	5849216	5842248	-10	108	3408	735	787	5847276	2214	1940	0.03%
$2p^53s$	1	5864770	5864502	5857770	-10	70	3303	708	784	5862626	2144	1876	0.03%
$2p^53s$	1	5960870	5960742	5953697	-10	74	3364	717	1042	5958883	1987	1859	0.03%
$2p^53d$	$^3P_1$	6471800	6471640	6466575	-11	16	2384	665	87	6469717	2083	1923	0.03%
$2p^53d$	$^3P_2$	6486400	6486183	6481385	-13	16	2250	658	86	6484383	2017	1800	0.03%
$2p^53d$	$^3F_4$	6486830	6486720	6482549	-12	27	1745	622	97	6485028	1802	1692	0.03%
$2p^53d$	$^3F_3$	6493030	6492651	6488573	-14	26	1740	607	84	6491016	2014	1635	0.03%
$2p^53d$	$^1D_2$	6506700	6506537	6502481	-17	21	1696	627	88	6504895	1805	1642	0.03%
$2p^53d$	$^3D_3$	6515350	6515203	6511163	-18	18	1762	604	87	6513617	1733	1586	0.02%
$2p^53d$	$^3D_1$	6552200	6552503	6548550	-16	-3	1747	616	134	6551029	1171	1474	0.02%
$2p^53d$	$^3F_2$	6594360	6594309	6589977	-16	22	1729	629	335	6592676	1684	1633	0.02%
$2p^53d$	$^3D_2$	6600950	6600998	6596316	-17	14	1947	641	334	6599235	1715	1763	0.03%
$2p^53d$	$^1F_3$	6605150	6605185	6600744	-17	19	1803	610	343	6603501	1649	1684	0.03%
$2p^53d$	$^1P_1$	6660000	6660770	6656872	-8	-52	1743	619	288	6659462	538	1308	0.02%
3C-3D		13.3655	13.4234	13.4302	0.0009	-0.0061	-0.0005	0.0004	0.0191	13.4440	-0.0785	-0.0206	0.15%

TABLE IV. Contributions to the $E1$ reduced matrix elements $D(3D) = D(2p^6\ {}^1S_0 - 2p^5 3d\ {}^3D_1)$ and $D(3C) = D(2p^6\ {}^1S_0 - 2p^5 3d\ {}^1P_1)$ (in a.u.) and the ratio of the respective oscillator strengths R. See caption of Table III for designations. L and V rows compared results obtained in length and velocity gauges for the $[12spdfg]$ basis. All other results are calculated using the length gauge. Transition rates are listed in the last row in s^{-1}.

		$D(3C)$	$D(3D)$	Ratio
$[5spdf6g]$		0.33492	0.17842	3.582
$[5spdf6g]$	+Triples	0.33493	0.17841	3.583
	Triples	0.00001	-0.00001	
$[5spdf6g]$	$+1s^2$	0.33480	0.17849	3.577
	$1s^2$	-0.00012	0.00007	
$[12spdfg]$	L	0.33527	0.17884	3.573
	V	0.33551	0.17894	3.574
$+[12spdfg]$		0.00036	0.00042	
$+[17dfg]$		-0.00001	0.00001	
QED		-0.00017	0.00030	
Final		0.33498	0.17921	3.552
Recomm.				3.55(5)
Transition rate		2.238×10^{13}	6.098×10^{12}	

$D(3D) = D(2p^6\ {}^1S_0 - 2p^5 3d\ {}^3D_1)$ and $D(3C) = D(2p^6\ {}^1S_0 - 2p^5 3d\ {}^1P_1)$ and the ratio of the respective oscillator strengths

$$R = \left(\frac{D(3C)}{D(3D)}\right)^2 \times \frac{\Delta E(3C)}{\Delta E(3D)}$$

are listed in Table IV. The energy ratio is 1.01655.

We include a very wide range of configurations obtained by triple excitations from the basic configurations as well as excitations from the $1s^2$ shell and find negligible corrections to both energies and matrix elements as illustrated by Tables III and IV. These contributions are listed as "Triples" and "$1s^2$" in both tables. A significant increase of the basis set from $[5spdf6g]$ to $[12spdfg]$ improves the agreement of energies with experiment but gives a very small, -0.009, contribution to the ratio. We find that the weights of the configurations containing $12fg$ orbitals are several times higher than those containing $12spd$ orbitals, so we expand the basis to include more dfg orbitals. We also include $2s^2 2p^3 nd^3$ and $2p^5 nd^3$ configurations up to $n = 14$. The contributions to the energies of the orbitals with $n = 13 - 17$ are $3 - 5$ times smaller than those with $n = 6 - 12$, clearly showing the convergence of the values with the increase of the basis set. The effect on the ratio is negligible. The uncertainty of the NIST database energies, 3000 cm^{-1} is larger than our differences with the experiment. The energies from the revised analysis of Fe^{16+} spectra [19] are estimated to be accurate to about 90 cm^{-1} and the scatter of the differences of different levels with the experiment is reduced. The last line of Table III shows the difference of the $3C$ and $3D$ energies in eV, with the final value 13.44(5)eV. We explored several different ways to construct the basis set orbitals. While the final results with an infinitely large basis set and complete configurations set should be identical, the convergence properties of the different basis sets vary, giving about 0.04 difference in the ratio and 0.04 eV in the $3C - 3D$ energy difference at the $12spdfg$ level. Therefore, we set an uncertainty of the final value of the ratio to be 0.05. As an independent

TABLE V. Contributions to the 3C and 3D line strengths S and the 3C/3D oscillator strength ratios (energy ratio 1.01655 is used). Energies in eV, transition rates A in s^{-1} and natural linewidths Γ in meV are listed in the last three rows of the tables.

	$S(3C)$	$S(3D)$	Ratio
Small basis	0.11217	0.03183	3.582
Medium basis	0.11241	0.03198	3.573
Large basis	0.11240	0.03199	3.572
+ triple excitations	0.11241	0.03198	3.573
$+1s^2$ shell excitations	0.11233	0.03201	3.567
+QED	0.11221	0.03212	3.552
Final	0.1122(2)	0.0321(4)	3.55(5)
Energies (eV)	825.67	812.22	
A (s^{-1})	$2.238(4) \times 10^{13}$	$6.10(7) \times 10^{12}$	
Γ (meV)	14.74(3)	4.02(5)	

test of the quality and completeness of the current basis set, we compare the results for $D(3C)$ and $D(3D)$ obtained in length and velocity gauges for the $[12spdfg]$ basis, see rows L and V in Table IV. The difference in the results is only 0.001. The final results for the line strengths S and the 3C/3D oscillator strength ratio after several stages of computations are summarised in Table V, which clearly illustrates a very small effect of all corrections.

This work was supported in part by U.S. NSF Grant No. PHY-1620687 and RFBR grants No. 17-02-00216 and No. 18-03-01220.

B. Multiconfiguration Dirac-Hartree-Fock calculations

In the multiconfiguration Dirac-Hartree-Fock (MCDHF) method, similarly to the CI approach outlined in the previous section, the many-electron state is given as an expansion in terms of a large set of jj-coupled configuration state functions [see Eq. (3)]. In contrast to the CI calculations, in the case of MCDHF, the single-electron wave functions (orbitals) are self-consistently optimized. We use the method in one of its most recent implementations, namely, applying the GRASP2018 code package [20]. For the virtual orbitals, the optimization of the orbitals was done in a layer-by-layer approach, i.e. when adding a new layer of orbitals (in our case, orbitals in the same shell) in the configuration expansions, the lower-lying single-electron functions are kept frozen.

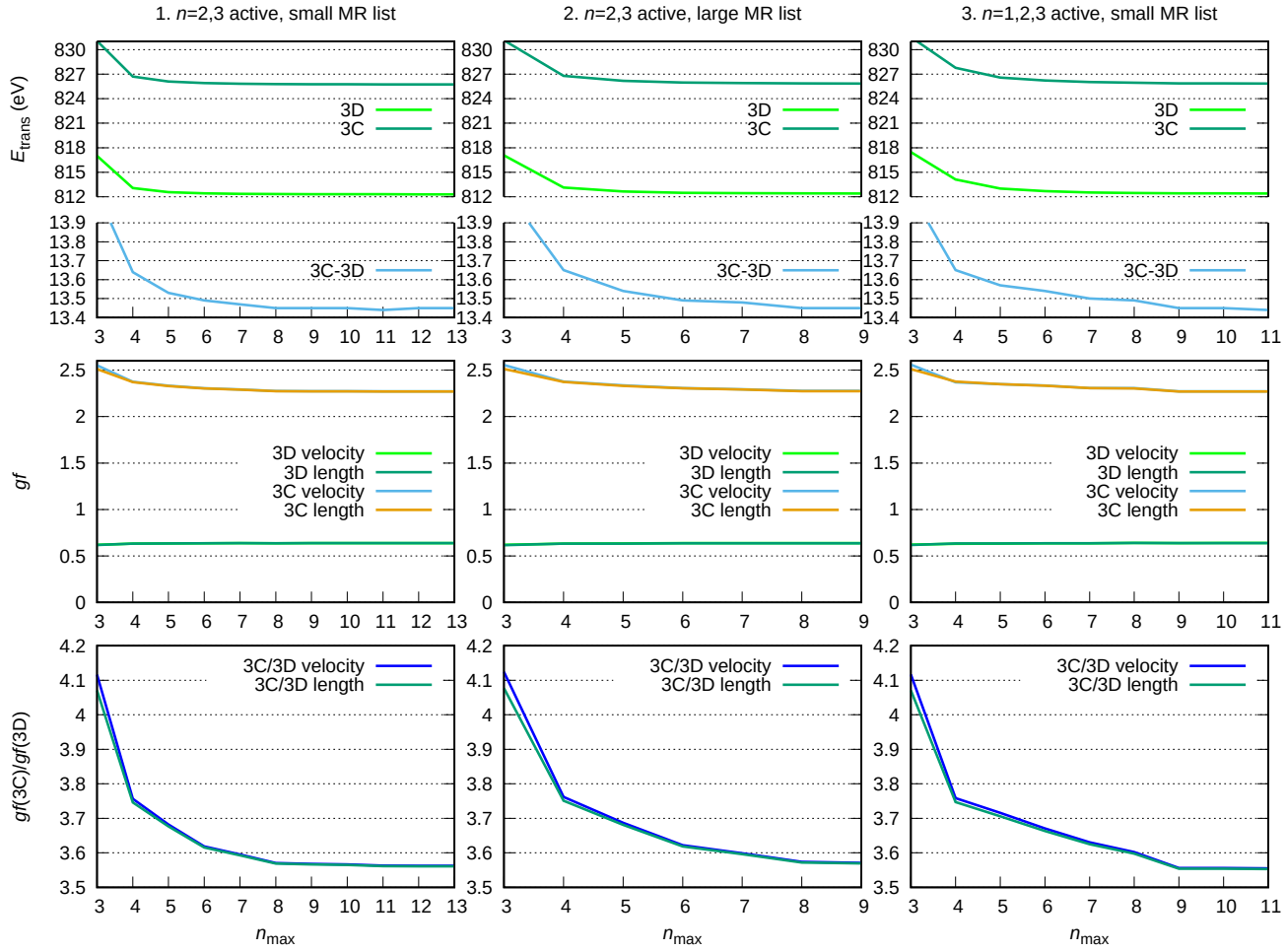

FIG. 4. Convergence of the MCDHF calculations: The X-ray transition energies of the 3C and 3D lines, their difference, the weighted oscillator strengths gf and their ratio vs. the maximal principal quantum number $n_{\max}$ used. Oscillator strengths are given both in the relativistic length (Babushkin) and velocity (Coulomb) gauges to numerically control gauge invariance. The different columns display results from different sets of calculations, as described in the text.

In a first set of calculations, we use the $2s^2 2p^6$ configuration for the ground state and the $2s^2 2p^5 3s$, $2s^2 2p^5 3d$, and $2s^1 2p^6 3p$ $J = 1$ odd configurations for the excited states to generate the configuration lists. Single and double electron exchanges from the $n = 2, 3$ spectroscopic (occupied) orbitals were taken into account up to virtual orbitals $n_{\max} spdfg$, where the maximal principal quantum number $n_{\max}$ is varied in the computations to study the convergence of the results. Such an approach is helpful in estimating the final theoretical uncertainty. Test calculations also using virtual orbitals with h and i symmetry have shown that these high angular momenta do not play a noticeable role. The ground and excited states were treated separately, i.e. two independently optimized sets of orbitals were used. After these multireference MCDHF calculations, the possible effects of further higher-order electron exchanges were included in a subsequent step, when a CI calculation was performed with the extended configuration lists (triple excitations from the multireference states up to $n = 4$ orbitals, yielding approx. 800 thousand configurations for $n_{\max} = 13$), employing the radial wave functions obtained from the previous MCDHF calculations. Furthermore, the effects of the frequency-independent Breit relativistic electron interaction operator, the normal and specific mass shift, and approximate radiative corrections are accounted for (see [20] and references therein). The QED effects have been included in the calculation of transition energies (which also enter the oscillator strengths), however, not in the electric dipole matrix elements, as such corrections are anticipated to be on the 1% level and thus can be neglected. The oscillator strengths were evaluated with the biorthogonal basis sets, each optimized separately for the ground- and excited states, to include orbital relaxation effects. The results of these calculations are presented in the first column of Fig. 4. The bottom panel shows that the oscillator strength ratio is converged from $n_{\max} = 9$ on.

In a subsequent set of calculations, the multireference set describing the ground and excited levels were expanded to include all $J = 0$ even and $J = 1$ odd states with 1 or 2 electrons in the M shell. The maximal principal quantum number of the virtual orbitals was set to 9 to limit the computational expense of calculations. Results are shown in the 2nd column of Fig. 4. In a third setting, calculations were performed with the smaller multireference list as described in the previous paragraph, however, with all spectroscopic orbitals (those with $n = 1, 2, 3$) included in the active set of orbitals when generating the configuration list. With the triple electron exchanges also included, this procedure yielded approx. 1.2 million configurations in the description of the excited states. The energies and strengths are shown in the last column of the figure. The converged 3C/3D oscillator strength ratios agree well for all 3 calculations. Comparing the different results, the final value for the ratio is 3.55(5), which agrees well with earlier large-scale MCDHF results [1, 21], and also with the results of the other theoretical methods described in this Supplement. For the difference of the energies of the 3C and 3D lines – which can be more accurately determined in the experiment than the absolute X-ray transition energies – we obtain 13.44(5) eV.

C. `AMBiT`: particle-hole CI method calculations

A separate CI calculation of the 3C and 3D lines in Fe^{16+} has been performed with the `AMBiT` code [22]. Our calculation begins with a Dirac-Hartree-Fock calculation of Ne-like Fe to construct the core $1s$, $2s$, and $2p$ orbitals in the V^N potential. The Breit interaction is included throughout the calculation. We diagonalize a set of B-splines in the Dirac-Fock potential to obtain valence orbitals. Configuration interaction is performed using the particle-hole CI method [23], however, this can be mapped exactly to the electron-only approach described in Section II A.

Our basic calculation is presented on the first line of Table VI. The CI space consists of all possible single and double excitations up to $10spdf$ from the same set of leading configurations presented previously: $2s^2\ 2p^6$, $2p^{-1}\ 3p$, $2p^{-1}\ 3s$, $2p^{-1}\ 3d$, $2p^{-1}\ 4d$, $2p^{-1}\ 5d$, and $2s^{-1} 3p$. At this stage, we do not include excitations from the frozen $1s^2$ core. Even for this calculation, the matrix size for the odd-parity $J = 1$ levels is $N = 479\,075$. To reduce the number of stored matrix elements we use emu CI [24], where interactions between high-lying configuration state functions are ignored. We limit the smaller side of the matrix to only including double excitations up to $5spdf$ and limit the number of $2s$ and $2p$ holes to single removals from an expanded set of leading configurations which include, in addition to those listed above, $2p^{-2}\ 3d^2$, $2p^{-1}\ 2s^{-1}\ 3d^2$, and $2s^{-2}\ 3d^2$. This results in a reduced small side $N_{small} = 80497$. We have checked that expanding the configuration state functions included in N_{small} makes no difference to our results at the displayed accuracy.

All of our calculations include the Breit interaction at all stages, and the dipole matrix elements are calculated in the relativistic formulation with $\omega = 30$ a.u. In the second and third lines of Table VI, we show the effects of removing the Breit interaction and using the static dipole matrix element ($\omega = 0$), respectively.

We then expand our calculation to include g-wave excitations, up to basis $10spdfg$. The difference from $10spdf$ is shown in the fourth line of Table VI. We see in the `AMBiT` calculation very little effect from the inclusion of these waves. In the fifth line, we show the effect of allowing excitations from $1s^2$, and in the sixth line we see the effect of including the Uehling potential [25] and self-energy [26] using the radiative-potential method [27]. This broadly agrees with the model-operator QED presented in Table IV.

The final row of Table VI gives the results including excitations to g-waves, excitations from $1s^2$, and QED effects.

The total number of configuration state functions accounted for is over 1.25 million for the odd-parity $J = 1$ symmetry. Nevertheless, the CI is not quite converged with respect to including orbitals with $n > 10$. We estimate based on calculations for $8spdf$ and $12spdf$ that the uncertainty in level energies is conservatively of order 3000 cm^{-1} and for the ratio gf_{3C}/gf_{3D} is of order 0.05. These results are consistent with the CI calculation presented in Sec. II A and the MCDHF results presented in Sec. II B.

TABLE VI. Particle-hole CI calculations using `AMBiT` of the level energies E_{3C} and E_{3D} (cm^{-1}), reduced matrix elements $D(3C)$ and $D(3D)$ (a.u.), and ratio of oscillator strengths of the $3C$ and $3D$ transitions in Fe^{16+}.

	E_{3C}	E_{3D}	$D(3C)$	$D(3D)$	gf_{3C}/gf_{3D}
$[10spdf]$	6661400	6552424	0.33893	0.17992	3.607
without Breit	6668847	6557636	0.33758	0.18164	3.511
$\omega = 0$			0.33937	0.18009	3.610
$+[10g]$	-15	-13	-0.000001	0.000003	
$+1s^2$	-103	-85	-0.000040	0.000016	
+QED	235	94	-0.00012	0.00031	
Final	6661517	6552420	0.33877	0.18025	3.591

[1] S. Bernitt, G. V. Brown, J. K. Rudolph, R. Steinbrugge, A. Graf, M. Leutenegger, S. W. Epp, S. Eberle, K. Kubicek, V. Mackel, *et al.*, Nature **492**, 225 (2012).
[2] C. R. Canizares, D. P. Huenemoerder, D. S. Davis, D. Dewey, K. A. Flanagan, J. Houck, T. H. Markert, H. L. Marshall, M. L. Schattenburg, N. S. Schulz, *et al.*, Astrophys. J. Lett. **539**, L41 (2000).
[3] C. Wu and X. Gao, Sci. Rep **9**, 7463 (2019).
[4] C. Shah, J. R. C. López-Urrutia, M. F. Gu, T. Pfeifer, J. Marques, F. Grilo, J. P. Santos, and P. Amaro, Astrophys. J. **881**, 100 (2019).
[5] M. F. Gu, Can. J. Phys. **86**, 675 (2008).
[6] P. Beiersdorfer, M. Bitter, S. Von Goeler, and K. Hill, Astrophys. J. **610**, 616 (2004).
[7] R. Blake, T. Chubb, H. Friedman, and A. Unzicker, Astrophys. J. **142**, 1 (1965).
[8] D. L. McKenzie, P. B. Landecker, R. M. Broussard, H. R. Rugge, R. M. Young, U. Feldman, and G. A. Doschek, Astrophys. J. **241**, 409 (1980).
[9] R. Mewe, A. J. J. Raassen, J. J. Drake, J. S. Kaastra, R. L. J. van der Meer, and D. Porquet, Astron. Astrophys **368**, 888 (2001).
[10] E. Behar, J. Cottam, and S. M. Kahn, Astrophys. J. **548**, 966 (2001).
[11] H. Xu, S. M. Kahn, J. R. Peterson, E. Behar, F. B. S. Paerels, R. F. Mushotzky, J. G. Jernigan, A. C. Brinkman, and K. Makishima, Astrophys. J. **579**, 600 (2002).
[12] Ness, J.-U., Schmitt, J. H. M. M., Audard, M., Güdel, M., and Mewe, R., A&A **407**, 347 (2003).
[13] J. Viefhaus, F. Scholz, S. Deinert, L. Glaser, M. Ilchen, J. Seltmann, P. Walter, and F. Siewert, Nucl. Instrum. Methods Phys. Res., Sect. A **710**, 151 (2013).
[14] `https://photon-science.desy.de/facilities/petra_iii/beamlines/p04_xuv_beamline/unified_data_sheet_p04/index_eng.html`.
[15] `https://photon-science.desy.de/facilities/petra_iii/beamlines/p04_xuv_beamline/beamline_parameters/index_eng.html`.
[16] I. I. Tupitsyn, M. G. Kozlov, M. S. Safronova, V. M. Shabaev, and V. A. Dzuba, Phys. Rev. Lett. **117**, 253001 (2016).
[17] V. A. Dzuba, V. V. Flambaum, and M. G. Kozlov, Phys. Rev. A **54**, 3948 (1996).
[18] A. Kramida, Yu. Ralchenko, J. Reader, and and NIST ASD Team, NIST Atomic Spectra Database (ver. 5.6.1), [Online]. Available: `https://physics.nist.gov/asd` [2019, September 6]. National Institute of Standards and Technology, Gaithersburg, MD. (2018).
[19] A. Kramida, Preliminary critical analysis of Fe XVII spectral data, Private Communication (2019).
[20] C. F. Fischer, G. Gaigalas, P. Jönsson, and J. Bieroń, Comput. Phys. Commun. **237**, 184 (2019).
[21] P. Jönsson, P. Bengtsson, J. Ekman, S. Gustafsson, L. Karlsson, G. Gaigalas, C. F. Fischer, D. Kato, I. Murakami, H. Sakaue, *et al.*, At. Data Nucl. Data Tables **100**, 1 (2014).
[22] E. V. Kahl and J. C. Berengut, Comput. Phys. Commun **238**, 232 (2019).
[23] J. C. Berengut, Phys. Rev. A **94**, 012502 (2016).
[24] A. J. Geddes, D. A. Czapski, E. V. Kahl, and J. C. Berengut, Phys. Rev. A **98**, 042508 (2018).
[25] J. S. M. Ginges and J. C. Berengut, J. Phys. B: At., Mol. Opt. Phys. **49**, 095001 (2016).
[26] J. S. M. Ginges and J. C. Berengut, Phys. Rev. A **93**, 052509 (2016).
[27] V. V. Flambaum and J. S. M. Ginges, Phys. Rev. A **72**, 052115 (2005).